Journal of Computational Science 55 (2021) 101446

Contents lists available at ScienceDirect

Journal of Computational Science

journal homepage: www.elsevier.com/locate/jocs

An automated platform for assembling light-powered hydrogel microrobots and their subsequent chemical binding

Jan Vrba [a,*], Charlie Maslen [a], Jana Maxova [a], Jan Duras [a], Ivan Rehor [a,b], Jan Mares [a]

[a] University of Chemistry and Technology Prague, Faculty of Chemical Engineering, Technická 5, Prague 6, 16628, Czech Republic
[b] Institute of Organic Chemistry and Biochemistry, Flamingovo Namesti 2, Prague, 16000, Czech Republic

ARTICLE INFO

Keywords:
Robotics
Image processing
Pattern recognition
Motion control
Microrobots
Hydrogel
PNIPAM
Radical crosslinking
Modular robotics

ABSTRACT

This paper presents light powered hydrogel microrobots (100 μm), that are directed to specific locations in their environment by an automated platform. The microrobots are actuated by focused laser light and crawl in aqueous environments by periodic volumetric changes of a section of their bodies. The platform consists of a stage, manipulated by stepper drivers and controlled by a Raspberry PI 4. This positions the laser light in the desired locations to move microrobots towards a goal location. The microrobots are localized via a microscope camera and repetitive usage of an algorithm based on Hough Gradient Method. The optimal position for the laser is chosen before every step so that the disk reaches the goal as fast as possible. Multiple disks are moved to form a formation of predefined geometry. An algorithm for finding the optimum sequence of disk movements to suitable positions is introduced. Subsequently, the disks are bound together chemically, using local UV illumination as the binding trigger. The bound formation can perform useful tasks, such as pushing and depositing a cargo at a target location.

1. Introduction

The development of micro-robotic systems that can perform useful work promises to advance technologies in a wide variety of fields just as conventional, human-scale robotics has transformed all industries in modern society. Microscopic scale robots can impart highly localized forces to their environment and, as such, hold great promise as tools for micro-manipulation, tissue engineering, or lab-on-chip studies [1,2]. To produce functional actuating robots on the microscopic scale (microrobots) requires a shift in the paradigm of what technologies are used. In order for microrobots to locomote, forces must be applied between their bodies and their environment. This can be realized in three significantly different ways. Through externally applied fields (e.g. magnetic fields [3]), through propulsion mechanisms (e.g. diffusiophoresis or bubble generation [4]), or through actuation cycles (e.g. swimming [5,6], crawling [7,8], or jumping [9]). Locomotion by actuation offers a greater diversity of motion behaviors and is a more direct analog of macroscopic robots. Conventionally, macroscopic robots are constructed from multiple components such as actuators, sensors and controllers. However, these components have a limit to how small they can be miniaturized and assembled. As such, current research is tending towards the use of alternative approaches, exploiting soft materials that can actuate by deformation in response to a stimulus such as light [10], magnetic field [11,12], or chemical changes in their environment [7]. These microrobots can locomote through an environment by cyclic periodic deformation of their bodies, and their navigation is provided by some external measurement system such as microscope imaging and control of the stimulus. Responsive hydrogels are candidate materials for microrobot production as they display different swelling behaviors in different environmental conditions such as pH, ionic strength, temperature, and chemical gradients. The swelling and deswelling property can be utilized to produce microscale actuators in micro-robotic, as well as sensing applications [7,13].

Different applications require distinct functionalities or designs of a microrobot. However, this brings the need to redraw production processes for each application and hence raises the cost and decreases the rate of production. As such, there is a demand for the development of modular micro-robotic systems that can be constructed 'in-the-field' to suit a desired application [13]. Modular robotics has been extensively researched for macro-scale robotics where unit robots connect to each other by mechanical interlocking [14,15] or magnetic attraction [16,17]. In the micrometer regime however, in which surface

The code (and data) in this article has been certified as Reproducible by Code Ocean: (https://codeocean.com/). More information on the Reproducibility Badge Initiative is available at https://www.elsevier.com/physical-sciences-and-engineering/computer-science/journals.

* Corresponding author.
E-mail addresses: Jan.Vrba@vscht.cz (J. Vrba), Ivan.Rehor@vscht.cz (I. Rehor).

https://doi.org/10.1016/j.jocs.2021.101446
Received 17 April 2021; Received in revised form 22 July 2021; Accepted 6 September 2021
Available online 30 September 2021

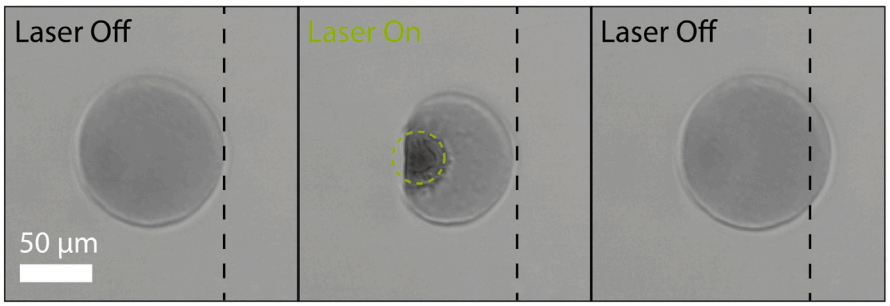

Fig. 1. Disk response to laser irradiation. After the irradiation pulse is complete, the disk displaces in the direction away from the laser.

forces dominate, alternative mechanisms can provide efficient connection of individual units, such as electrostatic attraction [18], depletion forces [19] or surface tension [20]. Furthermore, the use of polymeric materials, such as hydrogels, as a route to miniaturization also provides the possibility for chemical binding by covalent bond formation [21], coulombic interactions [18,22], or host-guest interaction [23,24].

In summary, despite the progress in micro-robotics, a robust system enabling construction of greater functional entities from individual locomoting microrobots as building blocks is yet to be presented. Furthermore, the practical application of such a system would require the building process to be autonomous and proceed without a direct intervention of the operator. In this research, we present crawling, disk-shaped hydrogel microrobots that are powered by absorption of focused laser pulses. The microrobots are driven by localized shrinking and expanding cycles coupled to a friction hysteresis between their bodies and surface [25]. The microrobots have full translational freedom owing to their radial symmetry, but individually display no additional functionalities besides locomotion. We developed a driving mechanism for the robots using image analysis coupled to a micropositioning system and pulsed focused irradiation. The disk-shaped robots are automatically navigated to a preassigned formation after which they are covalently bonded together forming a larger microrobot with different functionality. By then chemically binding them in a formation, they provide new abilities such as pivoting locomotion, and micromanipulation by guiding and releasing. We introduce an algorithm that optimizes the sequence of disk to target events in order to increase production rate, and eliminate the possibility of collisions.

2. Microrobots specification

2.1. Composition

The microrobots are composed of a thermo-responsive polymer – poly-*n*-isopropylacrylamide (PNIPAM) – cross-linked by poly(ethylene glycol) diacrylate (PEGDA). PNIPAM is a widely researched polymer owing to its thermo-responsive properties — at temperatures greater than 32 °C it transitions from a hydrophilic to a hydrophobic state. The hydrogel network, formed by cross-linking PNIPAM, thus de-swells reversibly when heated above 32 °C as water is expelled from the network. This is observed as isotropic contraction of the microgel to approximately 50% of the original volume. The stimulus inducing shrinking response can be transduced from heat, to visible light by incorporating gold nanospheres (15 nm) [26]. The nanoparticles absorb laser light at a resonant wavelength (532 nm) and photothermally heat the gel by plasmonic absorption. The shrinking response occurs rapidly and locally in the focal point of a focused 532 nm laser. Turning off of the laser and subsequent cooling of the network causes the gel to re-swell to its original volume.

2.2. Production

Microrobots are produced using a microgel synthesis technique, stop-flow lithography (SFL) [27,28], in which a photo-polymerizable pre-cursor solution is pumped into a microfluidic channel. The pressure is then removed, stopping the flow of pre-cursor. With the flow stationary, UV light is focused by a microscope objective on the channel through a photomask which induces radical polymerization and cross-linking of the pre-cursor — forming a hydrogel with shape given by the photomask. The thickness is given by the thickness of the channel (30 µm in our case). The pre-cursor used in this synthesis has a following composition:100 µL of gold colloid (aqueous dispersion, containing 1.5% w/w of 15 nm gold nanospheres [29]) is mixed with *n*-isopropylacrylamide (NIPAM) (37 mg), PEGDA (20 mg) and lithium phenyl-2,4,6-trimethylbenzoylphosphinate (LAP) (1.5 mg). 20 µl of methacryloxyethyl thiocarbonyl rhodamine B (10% in dimethyl sulfoxide) is added to allow disk visualization in scanning confocal microscopy. The pre-cursor is processed in SFL to produce 100 µm diameter disk-shaped microgels. Microfluidic channels are produced using poly-dimethylsiloxane (PDMS) molded from SU-8 on silicon photo-resists. After production, the microgels are stored in polystyrene wells with flat bottoms in a 1% Tween-20 surfactant solution. A glass slide is placed over the top of the well to remove any meniscus which would distort the laser beam.

2.3. Microrobots response to laser beam pulse

The microrobots are observed in the wells using an inverted microscope (Nikon Ti-U). A 200 mW 532 nm diode laser is reflected into the condenser lens of the microscope using a dichroic mirror (shortpass 480 nm). This allows for laser reflection and simultaneous diascopic observation. The condenser lens was used to focus the laser to a spot of approximately 30 µm diameter. Off-center irradiation of the disks leads to asymmetric shrinkage, and subsequent turning off of the light induces re-swelling. Coupled to a friction hysteresis between the shrinking and swelling domains, this leads to a displacement in the direction away from the center of irradiation (Fig. 1). Because the displacement always occurs along the line connecting the irradiation point and the disk center, full translational freedom is achieved by simply choosing the irradiation point. This point lies on a circle depicted in Fig. 2. The laser is turned on for a period of 900 ms to allow for complete contraction of the hydrogel. The laser is then turned off for a minimum of 2 s before a subsequent pulse, to allow for complete relaxation and translation of the microrobot.

2.4. Binding of adjacent microrobots

To covalently bind adjacent microrobots, they were deposited in wells containing a photoresponsive ‘binding’ solution. The solution is 20 µL PEGDA and 5 mg LAP in 475 µL aqueous Tween-80 (4%). To visualize the connection, the binding solution was made fluorescent by addition of 15 µl fluorescein O-methacrylate (30 mg/mL in dimethyl

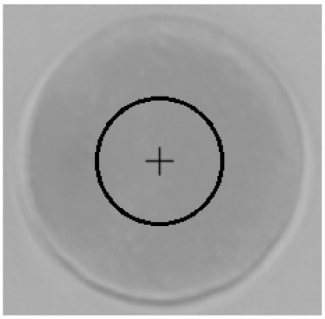

Fig. 2. Detailed photo of the disk-shaped microrobot with the proposed illumination regions that lies on the circle with center in the disks center (black cross) and radius 12 μm. The image is resized for better readability.

sulfoxide). Microrobots were then navigated to be in contact with the edge of another microrobot. UV-light is then focused through a circular photomask, placed in the beamstop of the microscope illuminating a region with diameter given by the mask, at the interface of the adjacent disks. This induces local gelation of the binding solution in this region, penetrating the networks of the microrobots and forming a covalent connection between them. The length of irradiation time was optimized to be 500 ms, and repeated pulses were used to establish a robust connection. A video of the process can be found in supplementary video 2. After 6× washings by fresh Tween solution, the fluorescently labeled PEGDA hydrogel connection was visualized using scanning confocal microscopy.

3. Automated platform overview

The platform consists of microscope with positioning stage, camera, step motors and laser, all controlled by Raspberry PI 4 and personal computer. The scheme of the system is depicted in the following Fig. 3 and the photo of the actual workplace is in Fig. 4.

The microscopes camera (DMK 23UX174) is connected to the personal computer (PC) via USB. It supports the adjustment of the brightness, gain, exposure and frames-per-second parameters. The acquired image has 2.07 megapixels with resolution 1920 × 1080 pixels. The focal point of the laser is fixed in relation to the camera which allows the position of the laser, with respect to the microrobots, to be controlled by the step motors positioning the stage. The x, y coordinates of the laser in the image and the goal are inputted manually and stored. The image is processed on the PC to obtain the positions of disks and calculate the desired number of steps to be done by the step motors in order to move the microrobot in the direction of the goal. The desired number of steps is sent to the Raspberry PI 4 via Ethernet, using a network socket. The stage is moved into the desired position for illumination, with the position of laser at the illumination region which will provide the greatest displacement towards the goal. The Raspberry PI 4 controls the TB6600 stepper drivers that are connected to NEMA17 step motors. Those steppers are connected via micrometric bolts to the stage, so precise positioning in two independent axes (X-axis, Y-axis) is achieved. When the movement is done, the laser pulse is performed, the microrobot displaces and an acknowledgment is sent to the PC. Then, the new image can be acquired and the result of the illumination is evaluated.

3.1. Software overview

In order to control the disk crawling and camera settings, a Python 3.7 [30] based software with graphical user interface was developed. A screenshot of the software is found in Fig. 5. The main functions of the software are:

- camera settings
- image processing
- laser-camera calibration
- setting the goal and disk to move
- saving the images and creating video sequences

All the image processing is done with NumPy [31] and OpenCV [32] libraries. The graphical user interface was created using PyQt5 [33] framework that enables portability between Windows/Linux machines. Multiple objectives (4×, 10×, 20× and 40×) for the microscope can be used with all parameters scaling.

3.2. Precision of the positioning

The NEMA17 step motors are controlled with a TB6600 driver in 1/4 micro-stepping mode. The 1/4 micro-stepping mode combined with the micrometric bolts of the stage allows precise positioning. Approximately 6.667 steps are required to change the location in the image by 1 pixel in the desired axis. This resolution is the same for both axes. The hardware design of the stage was inspired by that in Ref. [34].

3.3. Disk localization algorithm

For disk localization we used an algorithm based on Hough Gradient Method which is implemented in OpenCV 4.1 [32] as function $HoughCircles$ (HC). The HC in general perform two steps:

1. Find candidates for the center of circles
2. Find the optimum radius for each center candidate

Detailed description of an implemented algorithm can be found in [35]. As the noise in images is not significant and all disks are homogeneous with same radius that can be precisely estimated, it is a highly efficient approach that works at various magnifications with high accuracy (>99% successful detection in the range 4× to 40×) and low false-positives detection ($\ll$1%). The successful detection of disks via HC is depicted in Fig. 6.

3.4. Algorithm for formation establishing

As it is possible to move only one microrobot at a time, it is crucial to find the appropriate sequence for microrobots movements, as well as their suitable position in the formation. The aim is to avoid collisions between the microrobots and minimize the traveled distance. In order to meet these restrictions, we propose the following algorithm. Firstly, let's assume input and output of the algorithm as follows:

INPUT: $\mathcal{A} = \{A_1, \dots A_n\}$ distinct points in $\mathbb{R}^2$ (starting positions)
$\mathcal{B} = \{B_1, \dots B_n\}$ distinct points in $\mathbb{R}^2$ (target positions)

OUTPUT: 1) permutation that assigns a target position to each starting position
2) permutation that determines the order of moves whilst avoiding collisions between microrobots

Assume the following observation. All movements of the robots take place only in the convex hull of the points from $\mathcal{A} \cup \mathcal{B}$.

From this observation we immediately understand that:

1. If there is a target position $B^* \in \mathcal{B}$ such that B^* is not contained in the convex hull of the points from $\mathcal{A} \cup \mathcal{B} \setminus \{B^*\}$ then we may reduce the size n of the problem in the following way. We set A^* to be the starting position that is closest to B^*. We first move the robot from A^* to B^* and then solve the problem for smaller sets $\mathcal{A} \setminus \{A^*\}$ and $\mathcal{B} \setminus \{B^*\}$. The fact that A^* is the closest starting position to B^* guarantees that we avoid collision when moving the robot from A^* to B^*. The fact that B^* is not contained in the convex hull of the points from $\mathcal{A} \cup \mathcal{B} \setminus \{B^*\}$ guarantees that B^* will not cause any collision in the future.

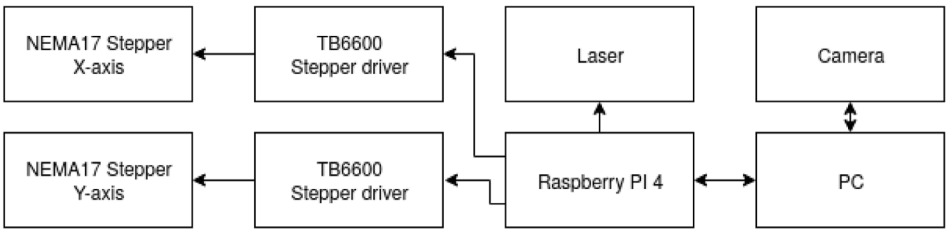

Fig. 3. The block diagram of the automated platform for the microrobots manipulation.

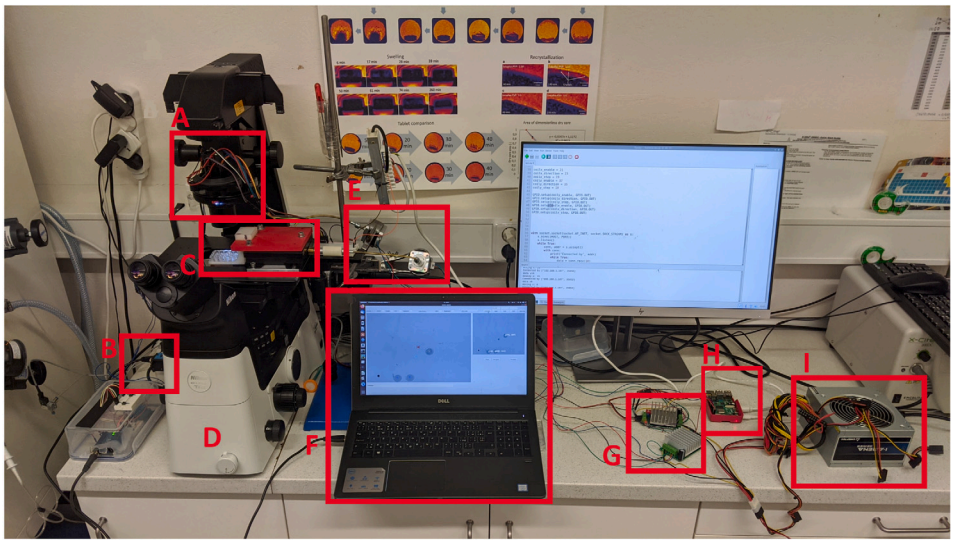

Fig. 4. The photo of the workplace with automated platform for microrobot manipulation. A - laser, B - camera, C - movable stage with wells containing microrobots, D - microscope, E - NEMA17 steppers, F - personal computer with running software, G - TB6600 drivers, H - Raspberry PI 4, I - ATX power supply used for powering TB6600 drivers.

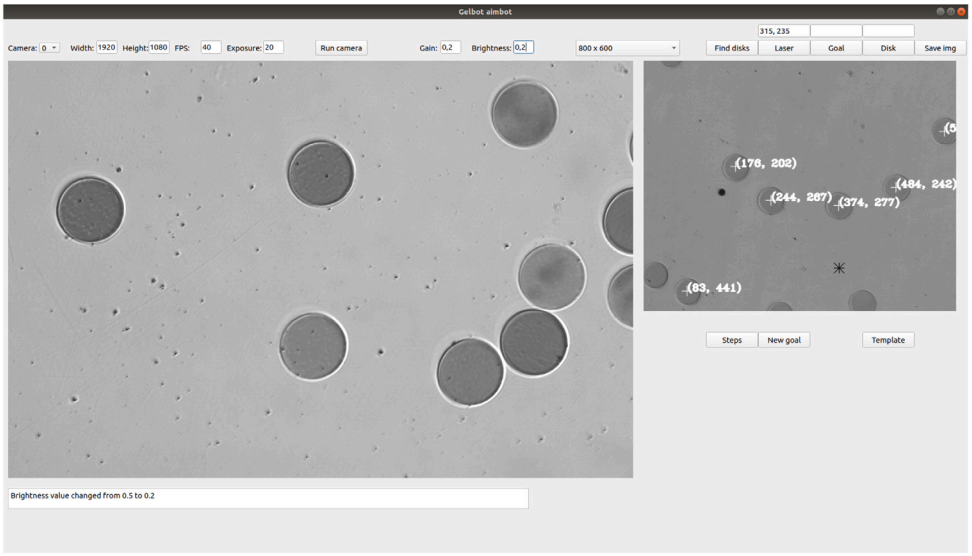

Fig. 5. The screenshot from the developed software for the automated platform for microrobot manipulation.

2. If there is a line $y = mx + b$, such that the number of starting positions (x, y) that satisfy $y \leq mx + b$ is the same as the number of target positions (x, y) that satisfy $y \leq mx + b$, then we may solve the problem in the half-plane $\{(x, y) \mid y \leq mx + b\}$ and in the half-plane $\{(x, y) \mid y > mx + b\}$ independently.

Resulting algorithm in $\mathbb{R}^2$

All points in $\mathcal{A} \cup \mathcal{B}$ lie in a real plane. Let $\mathcal{M}$ be the set of slopes of all lines determined by all pairs of points from $\mathcal{A} \cup \mathcal{B}$. In other words, $\mathcal{M}$ is the set of all numbers $(y_2 - y_1) \cdot (x_2 - x_1)^{-1}$, $x_1 \neq x_2$, where $X = (x_1, x_2)$ and $Y = (y_1, y_2)$ are any two distinct points in $\mathcal{A} \cup \mathcal{B}$.

- **Step 1**
  As long as there is a target position $B^* \in \mathcal{B}$ such that B^* is not contained in the convex hull of the points from $\mathcal{A} \cup \mathcal{B} \setminus \{B^*\}$ then we repeat the following:

  1. We set A^* to be the starting position that is closest to B^*.

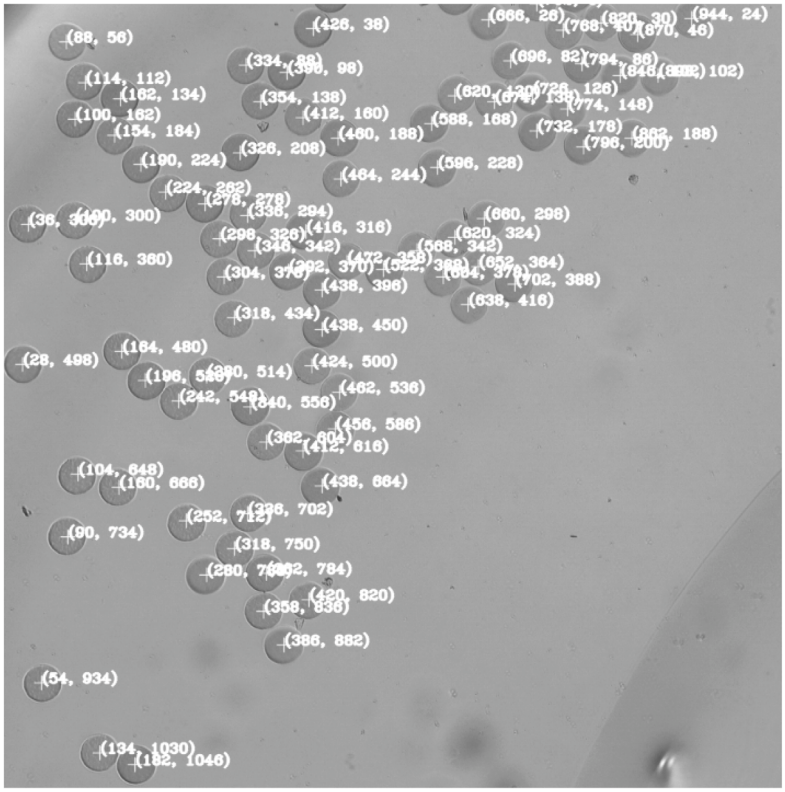

Fig. 6. The results of disk detection via HC. The white cross is placed in the center of disk. The centers coordinates are displayed to the right of it.

2. We move the robot from A^* to B^*.
3. We continue with $\mathcal{A} := \mathcal{A} \setminus \{A^*\}$ and $\mathcal{B} := \mathcal{B} \setminus \{B^*\}$.

- **Step 2**
  There is no target position $B^* \in \mathcal{B}$ such that B^* is not contained in the convex hull H of the points from $\mathcal{A} \cup \mathcal{B} \setminus \{B^*\}$. Thus the convex hull H is a k-gon whose vertices lie only in $\mathcal{A}$. We fix a real number m such that $m \in \mathbb{R} \setminus \mathcal{M}$. This is possible as the set $\mathcal{M}$ is finite, clearly $|\mathcal{M}| \leq \binom{2n}{n}$ where n represents the number of starting positions (equal to the number of target positions). Now we consider lines $y = mx + b$, $b \in \mathbb{R}$ with the given slope m. Let b_1 be the smallest real number b such that the line $y = mx + b$ intersects the convex hull H. Let us denote this line by L_1, i.e. $L_1 = \{(x, y) \mid y = mx + b_1\}$. Clearly, due to the choice of m, L_1 intersects the convex hull H in only one of its vertices, thus $L_1 \cap H \in \mathcal{A}$. Similarly, let b_2 be the biggest real number b such that the line $y = mx + b$ intersects the convex hull H. Let us denote this line by L_2, i.e. $L_2 = \{(x, y) \mid y = mx + b_2\}$. Again, due to the choice of m, the intersection $L_2 \cap H \in \mathcal{A}$. Note, that those two parallel lines forms a strip that contains all starting positions. Now we are ready to find a dividing line $y = mx + b$. We gradually change the value of b from b_1 to at most b_2 until the number of starting positions that satisfy $y \leq mx + b$ is the same as the number of target positions that satisfy $y \leq mx + b$. This is always possible, as the choice of m guarantees that for any b there is at most one point (x, y) from $\mathcal{A} \cup \mathcal{B}$ that satisfies $y = mx + b$. Now we solve the problem in the half-plane $\{(x, y) \mid y \leq mx + b\}$ and in the half-plane $\{(x, y) \mid y > mx + b\}$ independently. Note that this procedure can be also viewed as searching for translation of a boundary line L_1 to obtain two half-planes where the problem can be solved independently.

The proposed algorithm thus finds the desired order of disk movements to their according targets.

3.5. Automated control of formation making

The overall function of the automated platform for microrobot formation making can be described by the following algorithm.

Algorithm 1: workflow of the automated platform

```
user sets laser coordinates
user selects microrobots and position in desired formation
the sequence of microrobots movements to according position is
  found via algorithm for formation establishing (Section 3.4)
for microrobot and goal do
    while goal not reached do
        select the optimal region of target microrobot for laser
          illumination (equations 1, 2, 3)
        set the laser to desired position by moving steppers
        pulsed irradiation with the laser
        evaluate new position of target microrobot
        recompute all microrobots coordinates and their goals
    end
end
```

The user must calibrate laser coordinates in the image, choose the goals in formation and select the microrobots that will take the positions in the formation. All other steps are performed automatically. The coordinates region i.e. where the microrobot is illuminated by the laser, is estimated as follows:

$$k = \frac{y_g - y_d}{x_g - x_d + \epsilon} \tag{1}$$

$$x_l = x_d \pm \frac{r}{\sqrt{1 + k^2}} \tag{2}$$

$$y_l = k \cdot (x_l - x_g) + y_g \tag{3}$$

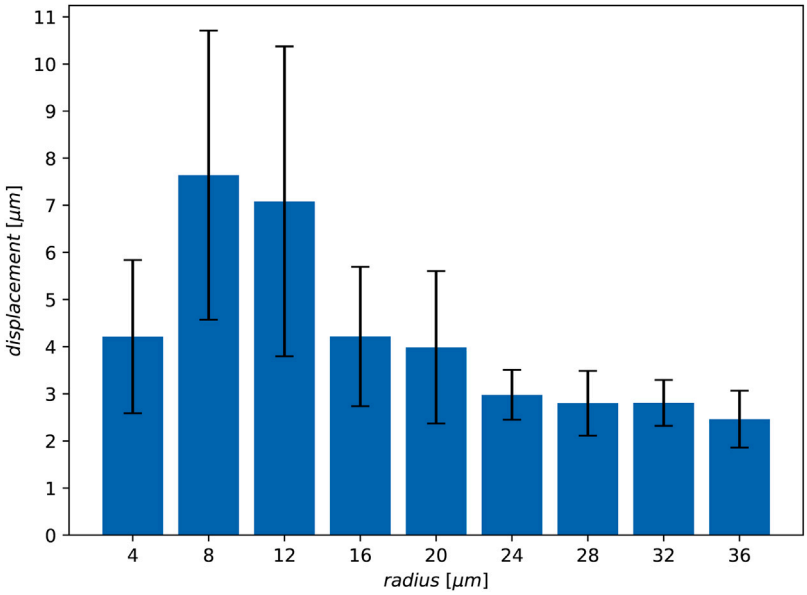

Fig. 7. Average displacement towards the target position, plotted against the radius within the disk at which the laser is targeted.

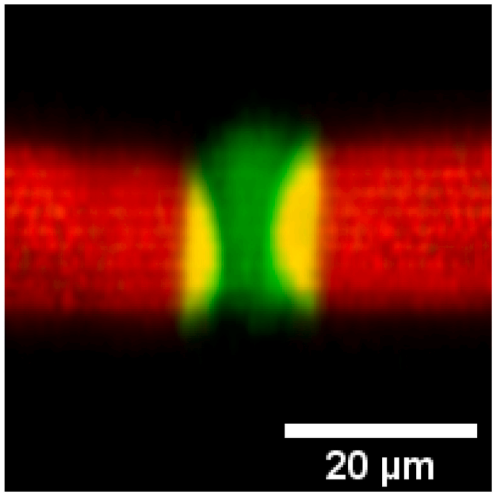

Fig. 8. Side on view of the microrobots (labeled red) and the PEGDA (labeled green) connection that binds them.

Where x_g is x coordinate of the goal, x_d is the x-axis coordinate of target disk, x_l is desired x-axis coordinate of the laser, y_g is y-axis coordinate of the goal, y_d is the y-axis coordinate of target disk and y_l is desired y-axis coordinate of the laser and r is desired distance of laser illumination point from the center of disk. The ϵ represents some small number to avoid division by zero. So the laser illumination point always lies in the intersection of the circle, that is given by the center of disk and radius r, and the line that is given by disk center and goal position. Note that Eq. (2) provides two values of x_l that results in two corresponding values of y_l so from two pairs of computed coordinates, the pair that is more distant from a desired goal has to be chosen for laser illumination coordinates.

4. Results and discussion

To induce crawling, the disk was irradiated at the position between its center and the opposite edge than the desired crawling direction. To achieve efficient locomotion, we first performed a systematic study on the dependency of the disk net displacement per one step on the irradiation position. Multiple disks were actuated with the laser positioned in a range of offsets from 4 μm to 48 μm (the edge of the disk), with randomly selected directions. The resulting step sizes as a function of the laser position can be seen in Fig. 7. As is clearly shown, the optimal radius for fast locomotion is 8 μm. At these smaller radii, the step sizes increase, however, the direction of the resulting step-size becomes more unpredictable which reduces the efficiency. As is shown, illumination at radius < 8 μm and radius > 32 μm induces only small displacements. However, the large radius positions can be exploited for more precise positioning of disks, as these display low average step sizes with relatively small standard deviation, in the direction towards the target.

The large errors are caused by various underlying phenomena present in the system. For example, convective flows arising from the local heating of the fluid may perturb the system. This effect was minimized by using shallow (0.3 mm) wells and providing sufficient times for the heat to dissipate. Another potential reason is local defects on the surface of the microrobots or the polystyrene surface. These may be present before use, or can be produced during the synthesis or binding processes. Still, with the laser positioned at 8 μm from the center of the disk, step sizes of approx. 7.5 μm, i.e 7.5% of the microrobot body, can be achieved. With laser pulses of 0.9 s and relaxation times of 2 s, the microrobots can navigate at 1.5 body-lengths per minute. We previously performed a similar study on position vs. step size on rectangular microrobots in Tween 20 (0.5%) solution [25]. Here, we performed the study with disks in the binding solution, containing PEGDA and photoinitiator. This solution increases the strength of the interaction between the disk and the surface, which is difficult to compensate for by changes in the surfactant (Tween 80) concentration. A video of the microrobots crawling into formation can be found in supplementary video 1.

Connection of adjacent microrobots was realized by localized gelation of the binding solution and was confirmed by confocal microscopy. In Fig. 8, it can be seen that the localized UV irradiation produces a small volume of PEGDA hydrogel. This can either penetrate within the microrobots or be a bridge connecting adjacent disks. The shape of the cross-linked PEGDA region is given by the dimensions of the photomask and the numerical aperture of the microscope. Furthermore, the connections can be attained even with microrobots that are not entirely adjacent to one another. This however results in a slightly mechanically less robust bond between the robots.

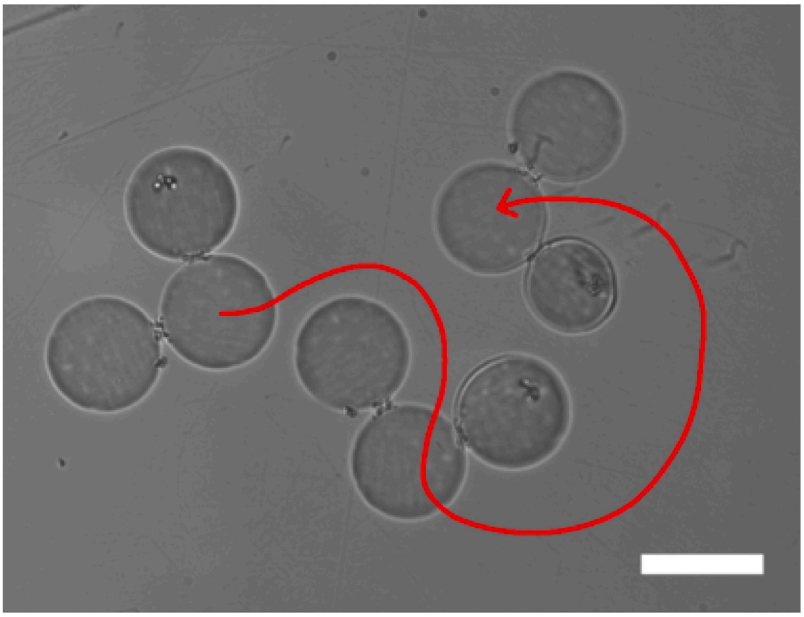

Fig. 9. An overlay montage of the pivoting motion for 3 microrobots bound into a V shape formation. The microrobot is able to navigate forwards and make complete turns. Scale bar is 100 μm.

The size of the circular illuminated region, determined by the size of the photomask was tested for a range of sizes (6.75, 12.5, 25, 50 μm diameter, as well as global irradiation). When subjected to UV illumination in the presence of a photoinitiator, remnant acrylate groups within the network of the microrobots become radicalized and form new cross-links between each other. This increases the cross-linking density which, in turn, shrinks the hydrogels permanently and proportionally to the duration and intensity of the illumination. As such, illuminating the contact region of two adjacent microrobots caused them to shrink away from each other, and any hydrogel produced could not bind them together. With smaller illumination regions, this effect is minimized and robust connections were only established with the 6.75 and 12.5 photomasks. As the effect was reduced for smaller regions, 6.75 μm was used as the standard for the remaining tests.

The PEGDA crosslinker concentration in the binding solution should be kept as low as possible to minimize the hindrance of crawling. However, it must be sufficient to induce gelation after crosslinking. This minimum concentration was found experimentally to be 3%, below which, no gel was formed under irradiation. Binding using only the remnant acrylates present in the microrobots was tested by illumination presence of only photo-initiator and no PEGDA. This did cause macroscopic shrinking of the illuminated regions, as the acrylate groups cross-linked with themselves, however, groups between the microrobots did not cross-link and no connection between the microrobot was established. A concentration of 4% PEGDA was established as the concentration which reliably produced robust connections, whilst also allowing crawling.

Both the intensity and duration of the UV illumination had similar effects on the resulting structure. At high intensity or long duration, the hydrogel produced would be prone to sticking to the polystyrene surface, disabling the microrobot. Furthermore, this effect would lead to long (approx. 100 μm), cylindrical structures growing in the z-direction from the focal point of the UV. This is attributed to the increased volume in which the radical concentration is increased above the gelation point, as well as to the escape of radical species from the focal volume transported away by convective and diffusive flows. At 4 W/cm^2 intensity and 500 ms of illumination these effects are rarely seen, and reducing either results in less robust connections.

Under the aforementioned conditions, and using a 20× objective with numerical aperture 0.5, the binding process produces a prolate spheroid of crosslinked PEGDA with a width approx. 10 μm and height 18 μm (Fig. 8). This height is smaller than the thickness of the crawler and does not affect their crawling by lifting the disk off the surface. However, this effect did occur when focusing the UV beneath the microrobots. In such cases, the PEGDA crosslinks and then swells, raising the bottom surface of the microrobot above the substrate and negating the friction dependent crawling mechanism.

In the next section, we demonstrate a proof-of-concept experiment, where individual disk-shaped microrobots are automatically navigated into a formation and subsequently bound together. A V-shaped microrobot is constructed from 2 disks joined to a 3rd at 90° from each other. Actuation of one leg drives the body forwards in an arcing trajectory (Fig. 9). Alternating which legs are actuated enables microrobot steering. By this, the front section of the microrobot can be navigated and pointed at a target which is impossible to achieve with singular disk microrobots. A video can be found in supplementary video 3.

We produced a Y-shaped microrobot consisting of 3 disks, joined around a 4th at intervals of 120° (Fig. 10). We assumed that this confines the translational motion to only 3 directions, however, a steering mechanism was discovered by illuminating the 'driving' disk at specific regions. The exact mechanism for this phenomenon requires further investigation. The design of the Y-shaped microrobot provides a collecting and depositing region which can be used for manipulation of objects. The microrobot is navigated using the three disks and the steering mechanism to a target, unattached disk. This disk can be subsequently pushed, firmly held between the two non-actuating disks on the microrobot. It can then be deposited by irradiation of the front of the central disk. This pulls the two front-most disks together, squeezing the manipulated disk out of the capturing region, and the microrobot can then be navigated away. A video of the entire process can be found in supplementary video 4.

5. Conclusions

For disk detection the algorithm based on Hough Gradient Method that is implemented in OpenCV 4.1 function $HoughCircles$ was used. It significantly increased the accuracy of detection (>99) while maintaining a low false-positive detection of disks ($\ll$1%) compared to our previous pattern matching approach [36]. We experimentally verified

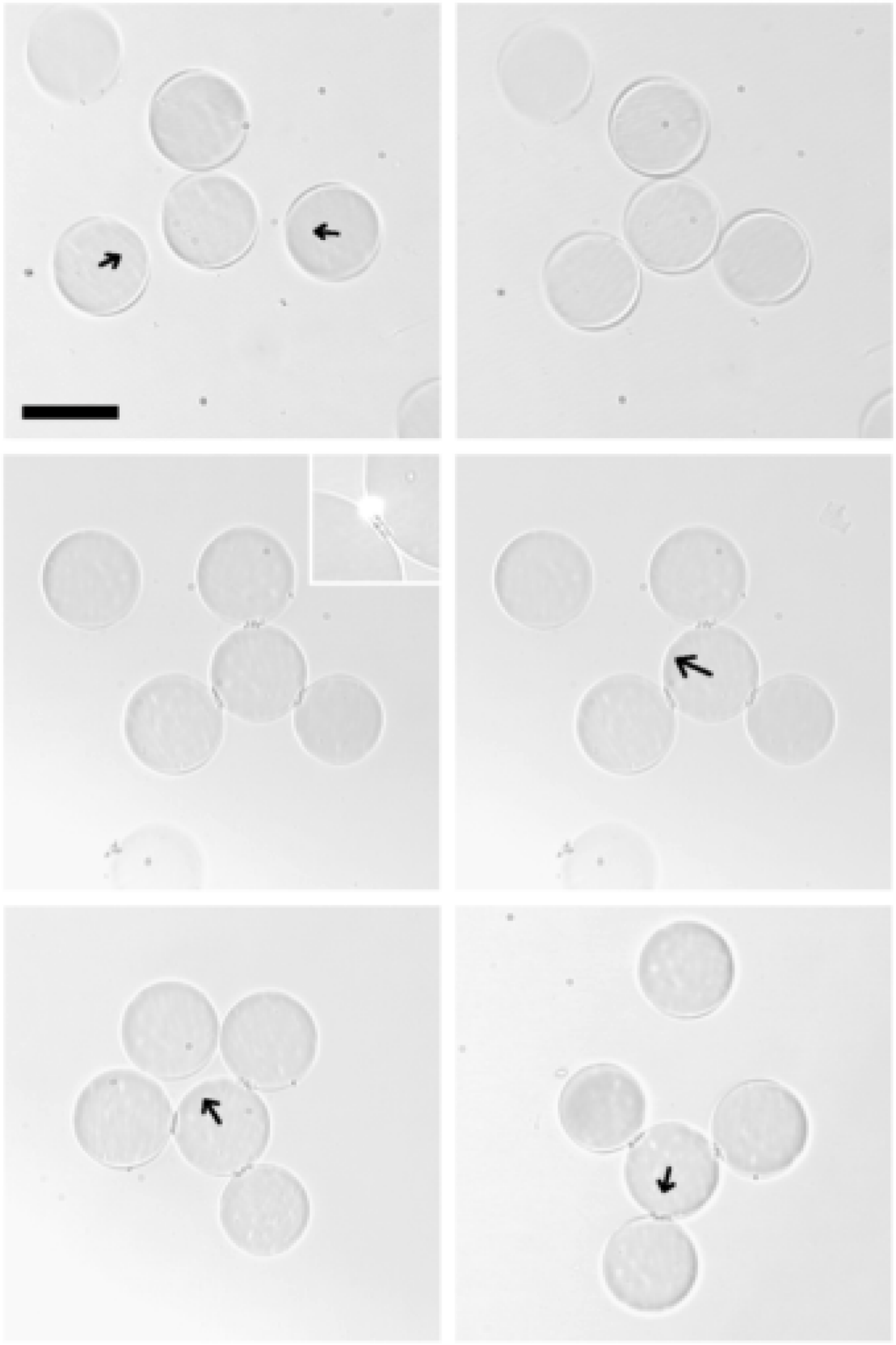

Fig. 10. The 'Y' shaped microrobot being assembled and used to manipulate and deposit a cargo disk. Scale bar is 100 μm.

that the proposed algorithm for collision-less formation making is suitable for the described application with disk microrobots. We developed a method for covalently binding micro-scale hydrogel objects, and used this to bind the formations, forming functional microrobots.

CRediT authorship contribution statement

Jan Vrba: Software, Writing – original draft, Writing – review & editing, Visualization, Formal analysis. **Charlie Maslen:** Validation, Investigation, Writing – original draft, Writing – review & editing, Funding acquisition. **Jana Maxova:** Methodology, Writing – original draft, Formal analysis. **Jan Duras:** Investigation. **Ivan Rehor:** Conceptualization, Supervision, Project administration, Writing – review & editing, Resources, Funding acquisition. **Jan Mares:** Resources, Writing – original draft, Funding acquisition.

Declaration of competing interest

The authors declare that they have no known competing financial interests or personal relationships that could have appeared to influence the work reported in this paper.

Acknowledgments

J. Vrba and C. Maslen contributed equally to this work. Financial support from specific university research, Czech Republic (MSMT No 21-SVV/2020). Financial support from MEYS INTER-EXCELLENCE project, Czech Republic LTAIN19007. UCT Institutional Support of 'Marie Prochazkova, Czech Republic'. Financial support from Junior GACR, Czech Republic project nr. 18-19170Y. C. Maslen was supported by the grant of Specific University Research, Czech Republic (Grant no. A1_FCHI_2020_005IG and A1_FCHI_2020_005). I. Rehor acknowledges his J.E. Purkyne fellowship.

Appendix A. Supplementary data

Supplementary material related to this article can be found online at https://doi.org/10.1016/j.jocs.2021.101446.

References

[1] M. Sitti, H. Ceylan, W. Hu, J. Giltinan, M. Turan, S. Yim, E. Diller, Biomedical applications of untethered mobile milli/microrobots, Proc. IEEE 103 (2) (2015) 205–224.
[2] H. Ceylan, J. Giltinan, k. Kozielski, M. Sitti, Mobile microrobots for bioengineering applications, Lab Chip 17 (10) (2017) 1705–1724.
[3] S. Tasoglu, E. Diller, S. Guven, M. Sitti, U. Demirci, Untethered micro-robotic coding of three-dimensional material composition, Nature Commun. 5 (1) (2014) 1–9.
[4] P. Sharan, A. Nsamela, S.C. Lesher-Pérez, J. Simmchen, Microfluidics for microswimmers: Engineering novel swimmers and constructing swimming lanes on the microscale, a tutorial review, Small (2021) 2007403.
[5] S. Palagi, A.G. Mark, S.Y. Reigh, K. Melde, T. Qiu, H. Zeng, C. Parmeggiani, D. Martella, A. Sanchez-Castillo, N. Kapernaum, et al., Structured light enables biomimetic swimming and versatile locomotion of photoresponsive soft microrobots, Nature Mater. 15 (6) (2016) 647–653.
[6] O. Aydin, X. Zhang, S. Nuethong, G.J. Pagan-Diaz, R. Bashir, M. Gazzola, M.T.A. Saif, Neuromuscular actuation of biohybrid motile bots, Proc. Natl. Acad. Sci. 116 (40) (2019) 19841–19847.
[7] S. Maeda, Y. Hara, T. Sakai, R. Yoshida, S. Hashimoto, Self-walking gel, Adv. Mater. 19 (21) (2007) 3480–3484.
[8] M. Rogóż, H. Zeng, C. Xuan, D.S. Wiersma, P. Wasylczyk, Light-driven soft robot mimics caterpillar locomotion in natural scale, Adv. Opt. Mater. 4 (11) (2016) 1689–1694.
[9] H. Lee, C. Xia, N.X. Fang, First jump of microgel; actuation speed enhancement by elastic instability, Soft Matter 6 (18) (2010) 4342–4345.
[10] H. Zeng, P. Wasylczyk, D.S. Wiersma, A. Priimagi, Light robots: bridging the gap between microrobotics and photomechanics in soft materials, Adv. Mater. 30 (24) (2018) 1703554.
[11] T. Xu, J. Zhang, M. Salehizadeh, O. Onaizah, E. Diller, Millimeter-scale flexible robots with programmable three-dimensional magnetization and motions, Science Robotics 4 (29) (2019).
[12] W. Hu, G.Z. Lum, M. Mastrangeli, M. Sitti, Small-scale soft-bodied robot with multimodal locomotion, Nature 554 (7690) (2018) 81–85.
[13] S. Palagi, P. Fischer, Bioinspired microrobots, Nat. Rev. Mater. 3 (6) (2018) 113–124.
[14] R. Groß, M. Bonani, F. Mondada, M. Dorigo, Autonomous self-assembly in swarm-bots, IEEE Trans. Robot. 22 (6) (2006) 1115–1130.
[15] H. Wei, Y. Chen, J. Tan, T. Wang, Sambot: A self-assembly modular robot system, IEEE/ASME Trans. Mechatronics 16 (4) (2010) 745–757.
[16] J.W. Romanishin, K. Gilpin, D. Rus, M-blocks: Momentum-driven, magnetic modular robots, in: 2013 IEEE/RSJ International Conference on Intelligent Robots and Systems, IEEE, 2013, pp. 4288–4295.
[17] N. Bredeche, E. Haasdijk, A. Prieto, Embodied evolution in collective robotics: A review, Front. Robot. AI 5 (2018) 12.
[18] G. Ju, F. Guo, Q. Zhang, A.J. Kuehne, S. Cui, M. Cheng, F. Shi, Self-correction strategy for precise, massive, and parallel macroscopic supramolecular assembly, Adv. Mater. 29 (37) (2017) 1702444.
[19] U. Okabe, T. Okano, H. Suzuki, Self-assembly of artificially manufactured microcomponents using the entropic effect, Sensors Actuators A 254 (2017) 43–53.
[20] Y. Du, E. Lo, S. Ali, A. Khademhosseini, Directed assembly of cell-laden microgels for fabrication of 3D tissue constructs, Proc. Natl. Acad. Sci. 105 (28) (2008) 9522–9527.
[21] J.G. Fernandez, A. Khademhosseini, Micro-masonry: construction of 3D structures by microscale self-assembly, Adv. Mater. 22 (23) (2010) 2538–2541.
[22] Y.L. Han, Y. Yang, S. Liu, J. Wu, Y. Chen, T.J. Lu, F. Xu, Directed self-assembly of microscale hydrogels by electrostatic interaction, Biofabrication 5 (3) (2013) 035004.
[23] M. Nakahata, S. Mori, Y. Takashima, A. Hashidzume, H. Yamaguchi, A. Harada, pH-and sugar-responsive gel assemblies based on boronate–catechol interactions, ACS Macro Lett. 3 (4) (2014) 337–340.
[24] A. Harada, R. Kobayashi, Y. Takashima, A. Hashidzume, H. Yamaguchi, Macroscopic self-assembly through molecular recognition, Nature Chem. 3 (1) (2011) 34–37.
[25] I. Rehor, C. Maslen, P.G. Moerman, B.G. Van Ravensteijn, R. Van Alst, J. Groenewold, H.B. Eral, W.K. Kegel, Photoresponsive hydrogel microcrawlers exploit friction hysteresis to crawl by reciprocal actuation, Soft Robot. 8 (1) (2021) 10–18.
[26] S.R. Sershen, G.A. Mensing, M. Ng, N.J. Halas, D.J. Beebe, J.L. West, Independent optical control of microfluidic valves formed from optomechanically responsive nanocomposite hydrogels, Adv. Mater. 17 (11) (2005) 1366–1368.
[27] D. Dendukuri, S.S. Gu, D.C. Pregibon, T.A. Hatton, P.S. Doyle, Stop-flow lithography in a microfluidic device, Lab Chip 7 (7) (2007) 818–828.
[28] I. Rehor, S. van Vreeswijk, T. Vermonden, W.E. Hennink, W.K. Kegel, H.B. Eral, Biodegradable microparticles for simultaneous detection of counterfeit and deteriorated edible products, Small 13 (39) (2017) 1701804.
[29] G. Frens, Controlled nucleation for the regulation of the particle size in monodisperse gold suspensions, Nat. Phys. Sci. 241 (105) (1973) 20–22.
[30] G. Van Rossum, F.L. Drake, Python 3 Reference Manual, CreateSpace, Scotts Valley, CA, 2009.
[31] C.R. Harris, K.J. Millman, S.J. van der Walt, R. Gommers, P. Virtanen, D. Cournapeau, E. Wieser, J. Taylor, S. Berg, N.J. Smith, R. Kern, M. Picus, S. Hoyer, M.H. van Kerkwijk, M. Brett, A. Haldane, J. Fernández del Río, M. Wiebe, P. Peterson, P. Gérard-Marchant, K. Sheppard, T. Reddy, W. Weckesser, H. Abbasi, C. Gohlke, T.E. Oliphant, Array programming with NumPy, Nature 585 (2020) 357–362, http://dx.doi.org/10.1038/s41586-020-2649-2.
[32] G. Bradski, The OpenCV library, Dr. Dobb's J. Softw. Tools (2000).
[33] M. Summerfield, Rapid GUI Programming with Python and Qt: The Definitive Guide to PyQt Programming, first ed., Prentice Hall Press, USA, 2015.
[34] R.A. Campbell, R.W. Eifert, G.C. Turner, Openstage: a low-cost motorized microscope stage with sub-micron positioning accuracy, PLoS One 9 (2) (2014) e88977.
[35] G. Bradski, A. Kaehler, Learning OpenCV: Computer Vision with the OpenCV Library, O'Reilly Media, Inc., 2008.
[36] J. Vrba, C. Maslen, I. Rehor, J. Mares, An automated platform for microrobot manipulation, in: International Workshop on Soft Computing Models in Industrial and Environmental Applications, Springer, 2020, pp. 255–265.

Jan Vrba is an assistant professor at Department of Computing and Control Engineering at University of Chemistry and Technology Prague. He received his Ph.D. in Technical Cybernetics in 2021. His research focuses on signal processing and machine learning. He is a member of Research group of optimization and cybernetics.

Charlie Maslen is a Ph.D. student of Chemical Engineering at the University of Chemistry and Technology Prague. His research focuses on the development of responsive hydrogels that can be produced with micrometer scale resolution for use in micro-robotic systems. He has a Masters degree in Chemistry, completed at Utrecht University where his thesis topic led to a publication on the subject of light-responsive hydrogel micro-crawlers.

Jana Maxova is an assistant professor at Department of Mathematics at University of Chemistry and Technology Prague. She received her Ph.D. in Combinatorics and Discrete Mathematics at Charles University, Prague, in 2002. Her research interest is in graph theory and applications, molecular graphs, Wiener index, graph algorithms and discrete optimization.

Jan Duras received his Bachelors degree in Nano and Microtechnology in Chemical Engineering from the University of Chemistry and Technology Prague. His interests involve microscopic soft robotics and their modularization. He is currently applying for a following Masters programme in Chemical Engineering.

Ivan Rehor, In his research group at University of Chemistry and Technology, Ivan Rehor focuses on programmable soft micromaterials, which can serve as remotely controlled locomotive robots, microbarcodes for edible product labeling or building blocks, assembling into larger structures. Before he started his independent research career, he absolved a postdoc stay at Utrecht University, focusing on microscale fabrication and assembly of soft materials. Before he was focusing on biomedical applications of various inorganic nanomaterials such as nanodiamonds, gold or Titanium dioxide in both diagnostics and therapy.

Jan Mares is an associate professor, head of Department of Computing and Control Engineering Doc. Mares received Ph.D. in Technical Cybernetics, he became an associate professor in Machine and Process Control in 2017. He is the head of Research group of optimization and cybernetics and has previous experience with application of cybernetics and informatics in biomedicine.